

The cone-beam algorithm of Feldkamp, Davis and Kress preserves oblique line integrals

Thomas Rodet¹, Frédéric Noo², Michel Defrise¹

¹Dept. of Nuclear Medicine, Vrije Universiteit Brussel, AZ-VUB, B-1090 Brussels, Belgium

² Dept. of Radiology, University of Utah, Salt-Lake City, Utah.

March 9, 2004

Abstract

The algorithm of Feldkamp, Davis and Kress (FDK, [1]) is a widely used filtered-backprojection algorithm for three-dimensional image reconstruction from cone-beam (CB) projections measured with a circular orbit of the x-ray source. A well-known property of this approximate algorithm is that the integral of the reconstructed image along any *axial* line orthogonal to the plane of the orbit is exact when the cone-beam projections are not truncated. We generalize this result to oblique line integrals, thus providing an efficient method to compute synthetic radiographs from cone-beam projections. Our generalized result is obtained by showing that the FDK algorithm is invariant under transformations that map oblique lines onto axial lines.

1 Introduction

The algorithm of Feldkamp, Davis and Kress (FDK, [1]) was introduced in 1984 to reconstruct cone-beam (CB) projections measured with a circular orbit of the x-ray source around the object. Despite considerable progress in the theory of CB reconstruction (see e.g. [2]), and despite its approximate character, the FDK algorithm is still widely used, either in its original form, or in various extensions developed for improved accuracy [3] or for helical cone-beam CT [4, 5, 6]. Applications include cardiac CT, small animal imaging, or radiotherapy. This lasting popularity stems from the simplicity and ease of implementation of the algorithm and from its good robustness to the CB artefacts caused by the incompleteness of the circular orbit [7, 8]. The good accuracy of the FDK algorithm is often related to three well-known properties, which were derived in the original paper [1]:

1. The reconstruction is exact in the plane of the circular orbit of the x-ray source.
2. The reconstruction is exact for any object which is invariant for translations in the *axial* direction orthogonal to the plane of the orbit.

3. The integral of the reconstructed image along any *axial* line orthogonal to the plane of the orbit is exact, i.e. the value of that integral coincides with the value of the corresponding line integral of the actual object.

In this note, we generalize the latter property by showing that the FDK reconstruction also preserves the value of integrals along *oblique* lines that are not orthogonal to the circular orbit plane. This result provides additional insight into the accuracy of the FDK reconstructions and of synthetic projections¹ which can be calculated from these reconstructions. Although this property has never, to our knowledge, been mentioned, the very possibility of calculating oblique line integrals from circular CB data has previously been demonstrated by Chen, Patch, and Trofimov. Chen [9] reconstructs an oblique line integral by integrating the ramp filtered 3D Radon transform for all planes containing the line. The ramp filtered 3D Radon transform can be calculated for a given plane using any CB projection measured for a vertex located in the plane, by using Smith’s intermediate function [12]. In Patch [10], CB projections are synthesized for any vertex located within the disk defined by the circular orbit. The computation is achieved by solving John’s equation for the three-dimensional x-ray transform, using the measured projections as boundary values. In Trofimov [11], a theorem supporting the results in Patch, Chen and this paper was given without the specification of an algorithm for the effective computation of line integrals. In this paper we show that the FDK algorithm allows the computation of oblique line integrals. After introducing the FDK algorithm in section 2, we demonstrate in section 3 the invariance of this algorithm for some affine transformation. This serves in section 4 to prove the preservation of oblique line integrals when two conditions are satisfied:

- The cone-beam projections are not truncated,
- The angle between the line and the axial direction does not exceed a maximum value that will be specified in section 4.

2 The FDK algorithm

We consider the reconstruction of a smooth function f from CB projections measured for cone vertices on a centered circle in the plane $z = 0$. To locate points in the field-of-view, vector notations $\vec{r} = x\vec{1}_x + y\vec{1}_y$ will be used for the transaxial components, while the axial coordinate z will be written separately. Thus, we write the density function as $f(\vec{r}, z)$, and throughout the paper, \vec{r} will denote a vector orthogonal to the axis $\vec{1}_z$ of the scan.

We assume that the function f is smooth and vanishes outside the cylinder

$$\Omega_f = \left\{ (\vec{r}, z) \in \mathbb{R}^3 \mid \|\vec{r}\| \leq R_{FOV}, |z| \leq H_{FOV} \right\}. \quad (1)$$

The position of the cone vertex is

$$\vec{a}(\lambda) = R \vec{1}_w(\lambda) \quad \lambda \in [0, 2\pi) \quad (2)$$

¹Such as Digitally Reconstructed Radiographs (DRR) in Radiotherapy.

where λ is the angle describing the rotation of the cone vertex, $R > R_{FOV}$ is the radius of the orbit, and

$$\vec{\mathbf{I}}_w(\lambda) = \cos \lambda \vec{\mathbf{I}}_x + \sin \lambda \vec{\mathbf{I}}_y \quad (3)$$

is a unit vector pointing from the origin of the coordinate system towards the cone vertex.

We consider a flat area detector which rotates with the cone vertex. At angular position λ , the detector is parallel to the z -axis and to the vector $\vec{a}'(\lambda)$ tangent to the circle. To simplify the derivations, we assume that the distance from $\vec{a}'(\lambda)$ to the detector is R , i.e. the detector contains the rotation axis $\vec{\mathbf{I}}_z$. Detector pixels are located with cartesian coordinates u and v measured along two orthogonal unit vectors in the plane $\mathcal{D}(\lambda)$ containing the flat area detector:

$$\begin{aligned} \vec{\mathbf{I}}_u(\lambda) &= -\sin \lambda \vec{\mathbf{I}}_x + \cos \lambda \vec{\mathbf{I}}_y \\ \vec{\mathbf{I}}_v &= \vec{\mathbf{I}}_z \end{aligned} \quad (4)$$

Thus, u is the transaxial coordinate ("detector element") whereas v is the axial coordinate ("detector row"). The origin $(u, v) = (0, 0)$ is at the orthogonal projection of $\vec{a}'(\lambda)$ onto $\mathcal{D}(\lambda)$.

The CB projection for vertex position λ is the set of line integrals $g_{meas}(u, v, \lambda)$ connecting $\vec{a}'(\lambda)$ to points (u, v) in $\mathcal{D}(\lambda)$. Throughout the paper, we use modified data $g(\lambda, u, v)$ obtained by applying the usual FDK weight to the measured data:

$$g(\lambda, u, v) = \frac{1}{\sqrt{R^2 + u^2 + v^2}} g_{meas}(\lambda, u, v) = \int_0^\infty dl f(\vec{X}(\lambda, u, l), lv) \quad (5)$$

with $(u, v) \in [-u_D, u_D] \times [-v_D, v_D]$ and

$$\vec{X}(\lambda, u, l) = (1-l) R \vec{\mathbf{I}}_w(\lambda) + l u \vec{\mathbf{I}}_u(\lambda) \quad (6)$$

In practice the limits of the integral over l in equation (5) are of course finite, and are determined by the radius of the FOV. We assume below that the projections are not truncated, i.e. the shadow of the cylindrical FOV is always contained within the detector. This requires

$$u_D \geq u_{max} = \frac{R R_{FOV}}{\sqrt{R^2 - R_{FOV}^2}}, \quad v_D \geq v_{max} = \frac{R H_{FOV}}{R - R_{FOV}} \quad (7)$$

The FDK algorithm [1] is an empirical 3D extension of the standard 2D fan-beam filtered-backprojection algorithm [13]. The reconstructed image is given by a CB backprojection:

$$f^{FDK}(\vec{r}, z) = \frac{1}{2} \int_0^{2\pi} d\lambda \frac{R^3}{(R - \vec{r} \cdot \vec{\mathbf{I}}_w(\lambda))^2} g^F(\lambda, U, V) \quad \|\vec{r}\| < R \quad (8)$$

where

$$\begin{aligned} U &= U(\vec{r}, \lambda) = \frac{R \vec{r} \cdot \vec{\mathbf{I}}_u(\lambda)}{R - \vec{r} \cdot \vec{\mathbf{I}}_w(\lambda)} \\ V &= V(\vec{r}, z, \lambda) = \frac{Rz}{R - \vec{r} \cdot \vec{\mathbf{I}}_w(\lambda)} \end{aligned} \quad (9)$$

are such that the ray defined by λ, U, V contains the point (\vec{r}, z) . The filtered projections are given by

$$g^F(\lambda, u, v) = \int_{-u_{max}}^{u_{max}} du' h_R(u - u') g(\lambda, u', v) \quad (10)$$

This is a 1D convolution of each detector row $v = const.$ with the kernel $h_R(u)$ of the ramp filter (the inverse 1D Fourier transform of $|\nu|$).

The FDK reconstruction is defined only for $\|\vec{r}\| < R$ because the magnification weight in equation (8) is singular when $\vec{r} = \vec{a}(\lambda)$. In addition, $f^{FDK}(\vec{r}, z)$ vanishes outside a volume Ω_{FDK} limited by two conical surfaces:

$$f^{FDK}(\vec{r}, z) = 0 \text{ when } (\vec{r}, z) \notin \Omega_{FDK} := \left\{ (\vec{r}, z) \mid \|\vec{r}\| < R \text{ and } |z| < v_{max} \left(1 + \frac{\|\vec{r}\|}{R}\right) \right\} \quad (11)$$

This property is verified by noting that the filtering in equation (10) is done row by row, and that $|V(\vec{r}, z, \lambda)| \geq R|z|/(R + \|\vec{r}\|)$.

Feldkamp et al [1] show that their algorithm preserves the value of axial line integrals when the CB projections are not truncated (i.e. when equation (7) is satisfied). Specifically, they show that for any \vec{r}_0 with $\|\vec{r}_0\| < R$,

$$\int_{(\vec{r}_0, z) \in \Omega_{FDK}} dz f^{FDK}(\vec{r}_0, z) = \int_{-H_{FOV}}^{H_{FOV}} dz f(\vec{r}_0, z) \quad (12)$$

In the left hand side of this equation, the FDK reconstruction must be integrated over the whole support Ω_{FDK} , i.e. over the range

$$-v_{max} \left(1 + \frac{\|\vec{r}_0\|}{R}\right) \leq z \leq v_{max} \left(1 + \frac{\|\vec{r}_0\|}{R}\right) \quad (13)$$

Thus, in order to use equation (12), the computation of the FDK reconstruction must not be restricted to the cylindrical support Ω_f of the object, but must include all "artefacts".

3 Invariance of the FDK algorithm for some affine transforms

To extend the property (12) to oblique lines, we first prove in this section that the FDK algorithm is invariant for affine transformations which map the object function f onto a "sheared" object (figure 1)

$$f_s(\vec{r}, z) := f(\vec{r} + z \vec{s}, z) \quad (14)$$

for some vector $\vec{s} \in \mathbb{R}^2$ orthogonal to $\vec{1}_z$. Restrictions on the vector \vec{s} will be discussed later.

The weighted CB projections of f_s are obtained by inserting equation (14) into (5):

$$\begin{aligned} g_s(\lambda, u, v) &= \int_0^\infty dl f_s(\vec{X}(\lambda, u, l), lv) \\ &= \int_0^\infty dl f(\vec{X}(\lambda, u, l) + lv \vec{s}, lv) \\ &= S g(\lambda, S(u + v \vec{s} \cdot \vec{1}_u(\lambda)), S v) \end{aligned} \quad (15)$$

where S is the following function of λ and v :

$$S = S(v, \lambda) = \frac{R}{R - v \vec{s} \cdot \vec{1}_w(\lambda)} \quad (16)$$

To simplify notations, the arguments of S are omitted in most equations below. The last line in equation (15) is obtained by noting that $\vec{X}(\lambda, u, l) + lv \vec{s} = \vec{X}(\lambda, S(u + v \vec{s} \cdot \vec{1}_u(\lambda)), S^{-1}l)$, by changing the integration variable to $l' = S^{-1}l$, and by comparing the result with equation (5).

We now apply the FDK algorithm to the sheared data. The first step is the ramp filtering of each detector row, according to equation (10):

$$\begin{aligned} g_s^F(\lambda, u, v) &= \int_{-\infty}^{\infty} du' h_R(u - u') g_s(\lambda, u', v) \\ &= \int_{-\infty}^{\infty} du' h_R(u - u') S g(\lambda, S(u' + v \vec{s} \cdot \vec{1}_u(\lambda)), Sv) \end{aligned} \quad (17)$$

Setting $\tilde{u} := S(v, \lambda)(u' + v \vec{s} \cdot \vec{1}_u(\lambda))$, and using the scaling property $h_R(cu) = h_R(u)/c^2, c > 0$, we get

$$\begin{aligned} g_s^F(\lambda, u, v) &= \int_{-\infty}^{\infty} d\tilde{u} h_R(u - S^{-1}\tilde{u} + v \vec{s} \cdot \vec{1}_u(\lambda)) g(\lambda, \tilde{u}, Sv) \\ &= S^2 \int_{-\infty}^{\infty} d\tilde{u} h_R(S(u + v \vec{s} \cdot \vec{1}_u(\lambda)) - \tilde{u}) g(\lambda, \tilde{u}, Sv) \\ &= S^2 g^F(\lambda, S(u + v \vec{s} \cdot \vec{1}_u(\lambda)), Sv) \end{aligned} \quad (18)$$

The second step of the algorithm is the backprojection (8), yielding the reconstructed sheared image f_s^{FDK} :

$$\begin{aligned} f_s^{FDK}(\vec{r}, z) &= \frac{1}{2} \int_0^{2\pi} d\lambda \frac{R^3}{(R - \vec{r} \cdot \vec{1}_w(\lambda))^2} g_s^F(\lambda, U(\vec{r}, \lambda), V(\vec{r}, z, \lambda)) \\ &= \frac{1}{2} \int_0^{2\pi} d\lambda \frac{R^3}{(R - \vec{r} \cdot \vec{1}_w(\lambda))^2} S^2 \times \\ &\quad \times g^F(\lambda, S(U(\vec{r}, \lambda) + V(\vec{r}, z, \lambda) \vec{s} \cdot \vec{1}_u(\lambda)), SV(\vec{r}, z, \lambda)) \end{aligned} \quad (19)$$

with $S = S(V(\vec{r}, z, \lambda), \lambda)$. Noting the three relations,

$$\begin{aligned} \frac{S(V(\vec{r}, z, \lambda), \lambda)}{R - \vec{r} \cdot \vec{1}_w(\lambda)} &= \frac{1}{R - (\vec{r} + z \vec{s}) \cdot \vec{1}_w(\lambda)} \\ S(V(\vec{r}, z, \lambda), \lambda) (U(\vec{r}, \lambda) + V(\vec{r}, z, \lambda) \vec{s} \cdot \vec{1}_u(\lambda)) &= U(\vec{r} + z \vec{s}, \lambda) \\ S(V(\vec{r}, z, \lambda), \lambda) V(\vec{r}, z, \lambda) &= V(\vec{r} + z \vec{s}, z, \lambda) \end{aligned} \quad (20)$$

and comparing equations (19) to (8), one obtains

$$f_s^{FDK}(\vec{r}, z) = f^{FDK}(\vec{r} + z \vec{s}, z) \quad (21)$$

This concludes the proof that the FDK algorithm is invariant for the affine mapping (14). This results holds for any \vec{s}, \vec{r}, z such that $\|\vec{r}\| < R$ and $\|\vec{r} + z\vec{s}\| < R$ so that the FDK reconstructions in the left and right hand sides of equation (21) are defined. In view of the first line of equation (20), this condition also guarantees that $S(v, \lambda)$ is finite.

4 Preservation of oblique line integrals by the FDK algorithm

The property that the integral of the FDK reconstruction along an oblique line defined by $\vec{r} = \vec{r}_0 + z\vec{s}$ is exact is a direct consequence of the invariance property derived in the previous section. Indeed, we can write

$$\begin{aligned} \int_{-\infty}^{\infty} dz f^{FDK}(\vec{r}_0 + z\vec{s}, z) &= \int_{-\infty}^{\infty} dz f_s^{FDK}(\vec{r}_0, z) \\ &= \int_{-\infty}^{\infty} dz f_s(\vec{r}_0, z) \\ &= \int_{-\infty}^{\infty} dz f(\vec{r}_0 + z\vec{s}, z) \end{aligned} \quad (22)$$

where the first equality uses equation (21). The second equality follows from the fact that f_s^{FDK} is obtained by applying the FDK algorithm to the CB projections of f_s , and from the preservation of axial line integrals by this algorithm. The last equality is obtained using the definition of the mapping (14).

Let us now discuss the conditions of validity of our main result. Equation (22) assumes that the relation (21) holds for all points of the oblique line for which $f^{FDK}(\vec{r}, z) \neq 0$. This condition requires that the intersections of the oblique line with the boundaries of the support Ω_{FDK} of $f^{FDK}(\vec{r}, z)$ are both on the lower or upper conical surface (see equation (11)), and not on the lateral surface of the cylinder of radius R , where f^{FDK} is not defined. Hence the intersections of the oblique line of parametric equation $(\vec{r}_0 + z\vec{s}, z)$ with the cylinder of radius R must both be located at $|z| > 2v_{max}$. One easily checks that this condition is satisfied when $\|\vec{r}_0\| < R$ and

$$2\|\vec{s}\|v_{max} < \sqrt{R^2 - \|\vec{r}_0\|^2 + \frac{(\vec{r}_0 \cdot \vec{s})^2}{\|\vec{s}\|^2}} - \frac{|\vec{r}_0 \cdot \vec{s}|}{\|\vec{s}\|} \quad (23)$$

Equation (23) also implies that the support of the sheared object $f_s(\vec{r}, z)$ is contained within the cylinder of radius R , thus guaranteeing that $f_s^{FDK}(\vec{r}, z)$ is well-defined. To verify this statement, note that

$$f_s(\vec{r}, z) \neq 0 \rightarrow (\vec{r} + z\vec{s}, z) \in \Omega_f \rightarrow |z| \leq H_{FOV} \text{ and } \|\vec{r} + z\vec{s}\| \leq R_{FOV} \quad (24)$$

Therefore,

$$f_s(\vec{r}, z) \neq 0 \rightarrow \|\vec{r}\|^2 = \|\vec{r} + z\vec{s}\|^2 + \|\vec{s}\|^2 z^2 - 2z\vec{s} \cdot (\vec{r} + z\vec{s})$$

$$\begin{aligned}
&\leq R_{FOV}^2 + \left(\frac{R - R_{FOV}}{2H_{FOV}}\right)^2 H_{FOV}^2 + 2\frac{R - R_{FOV}}{2H_{FOV}} H_{FOV} R_{FOV} \\
&= \frac{(R + R_{FOV})^2}{4} < R^2
\end{aligned} \tag{25}$$

where we have used the fact that condition (23), with v_{max} from equation (7), implies $\|\vec{s}\| < R/(2v_{max}) = (R - R_{FOV})/(2H_{FOV})$. We finally conclude that equation (23) is a sufficient condition of validity for equation (22).

5 Conclusion

We have shown that the filtered-backprojection algorithm of Feldkamp, Davis and Kress for circular cone-beam reconstruction preserves the values of oblique line integrals, thereby generalizing the well-known property that axial line integrals are preserved. This property provides new insight into the accuracy of this widely used algorithm, and it also suggests an efficient way of calculating synthetic radiographs from CB data. The property only holds when the CB projections are not truncated and it requires an additional condition on the angle between the line and the axial direction. Its practical significance, therefore, mainly concerns the imaging of small animals and of isolated tissue samples, which can be put on blocks of material with very low attenuation to meet the hypothesis of non-truncation.

References

- [1] Feldkamp L A, Davis L C and Kress J W, 1984, Practical cone-beam algorithm, *J Opt Soc Am*, **A6**, 612-619
- [2] Katsevich A 2002, Improved exact FBP algorithm for spiral CT, subm. *Adv Appl Math*, see also: Analysis of an exact inversion algorithm for spiral cone-beam CT, *Phys Med Biol*, **47**, 2583-2597 (2002).
- [3] Grass M, Köhler T, Proksa R, 2000, 3D cone-beam CT reconstruction for circular trajectories, *Phys Med Biol*, **45**, 329-348
- [4] Kudo H and Saito T, 1992, Helical-scan computed tomography using cone-beam projections, *Conf. Rec. 1991 IEEE Med Imag Conf (Santa Fe, NM)*, 1958-1962
- [5] Wang G, Lin T H, Cheng P and Shinozaki D M, 1993, A general cone-beam reconstruction algorithm, *IEEE Trans Med Imag*, **MI-12**, 486-496
- [6] Yan X and Leahy R M, 1992, Cone-beam tomography with circular, elliptical and spiral orbits, *Phys Med Biol*, **37**, 493-506
- [7] Tuy H, 1983, An inversion formula for cone-beam reconstruction, *SIAM J Appl Math*, **43**, 546-552

- [8] Grangeat P, 1991, Mathematical framework of cone-beam 3D reconstruction via the first derivative of the Radon transform *Mathematical Methods in Tomography* (eds Herman G T, Louis A K, Natterer F), *Lecture Notes in Mathematics* (Berlin: Springer) **1497** 66-97
- [9] Chen J, 1992, A theoretical framework of regional cone-beam tomography, *IEEE Trans Med Imag*, **MI-11** 342-351
- [10] Patch S K, 2002, Consistency conditions upon 3D CT data and the wave equation, *Phys Med Biol*, **47**, 2637-2650. US Patent 6173030 (1999).
- [11] Trofimov O E, 2003, Virtual beam (X-ray) projections, Proceedings of the 2003 International Conference on Fully 3D Reconstruction in Radiology and Nuclear Medicine, Saint-Malo, France, June 2003. Ed. Y. Bizais.
- [12] Smith B D, 1985, Image Reconstruction from Cone-Beam Projections - Necessary and Sufficient Conditions and Reconstruction Methods, *IEEE Trans Med Imag*, **MI-4** 14-25
- [13] Natterer F, 1986, *The Mathematics of Computerized Tomography*, Wiley.

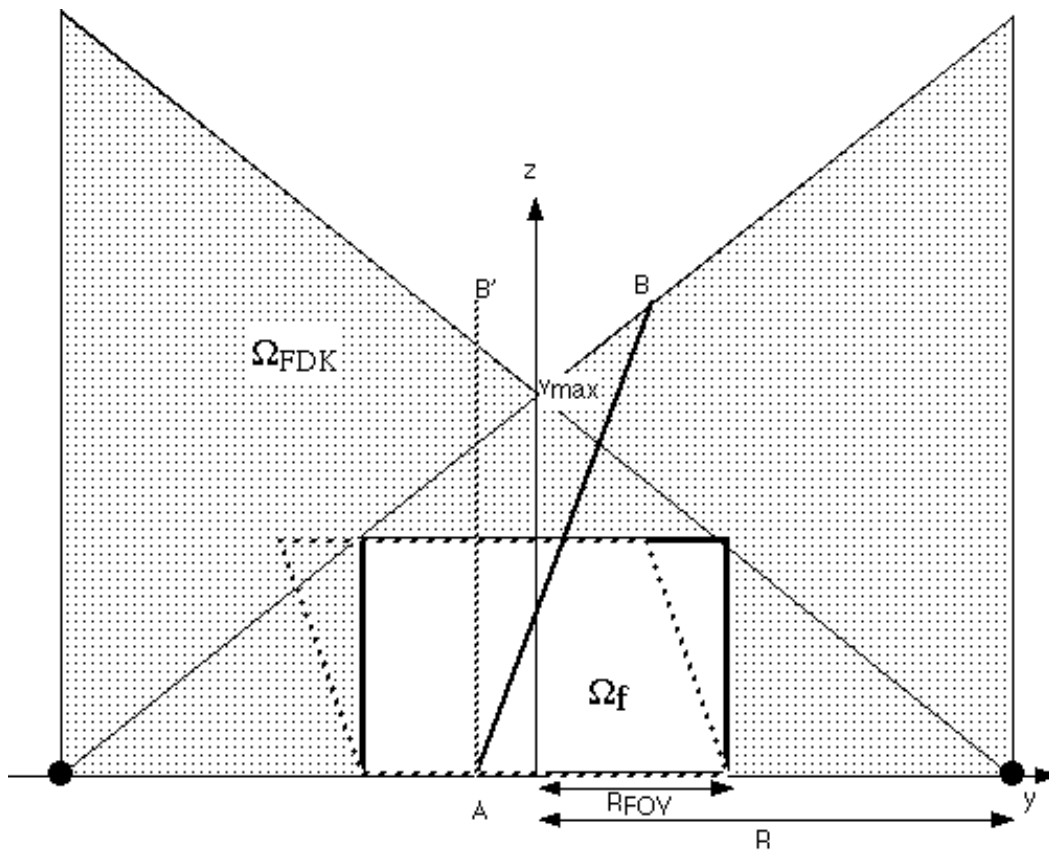


Figure 1: A longitudinal section of the object support Ω_f , also showing the intersection with the circular orbit (small black disks). Only the $z \geq 0$ region is shown, and non-truncated projections are assumed. The region Ω_{FDK} in which the FDK reconstruction of f is non zero is shown by the dotted pattern. The sheared object defined by the affine transform (14) is shown by the dashed parallelogram. The oblique line AB is transformed into the axial line AB' through the sheared object.